

Rotational Number Approach to a Damped Pendulum under Parametric Forcing

Eun-Ah KIM* and K.-C. LEE

Department of Physics, Seoul National University, Seoul 151-742

M. Y. CHOI

*Department of Physics, Seoul National University, Seoul 151-742 and
Korea Institute for Advanced Study, Seoul 130-722*

S. KIM†

*Nonlinear and Complex Systems Lab., Department of Physics and Asia Pacific Center for Theoretical Physics,
Pohang University of Science and Technology, Pohang 790-784*

(Received 8 October 2003, in final form 17 February 2004)

We study the dynamical behavior of a damped pendulum under parametric forcing, which exhibits various chaotic dynamics characterized by the rotation number: oscillating, rotating, and tumbling chaos. The analysis of the detailed bifurcation diagram together with the rotation number reveals the existence of multiple types of rotational onset. At relatively high forcing frequencies, the system successively undergoes a hysteretic rotational onset from oscillating chaos to periodic rotation due to bistability and a non-hysteretic onset from rotating chaos to tumbling chaos. The onset mechanism of the latter is found to result from an interior crisis and an attractor merging crisis. On the other hand, at relatively low forcing frequencies the system exhibits a direct non-hysteretic onset from periodic oscillation to tumbling chaos, arising from a tangency crisis. This reveals the complex structure of the phase diagram at low forcing frequencies.

PACS numbers: 05.45.+b

Keywords: chaos, Nonlinear dynamics, Rotation number

I. INTRODUCTION

The dynamical properties of a nonlinear pendulum have attracted much interest since the discovery of chaos under appropriate conditions. In particular, periodic displacement of the suspension point along the vertical direction leads to periodic variation of the effective gravitational field, and the resulting parametrically forced pendulum [1,2] models many physical systems including a magnetic pendulum under ac and dc magnetic field [3, 4], and related problems of Josephson junctions and neurons under stimuli [5–8]. Despite the apparent simplicity of the equation of motion, the parametrically forced pendulum is known to display rich dynamical behavior including chaos. For relatively weak forcing, the system was studied mostly by means of the Poincaré section, and period-doubling bifurcations to a small chaotic attractor were found both numerically [9,10] and analytically [11],

and were also observed in experiments [12,13]. As the forcing amplitude is increased further, the appearance of a transition to a large chaotic attractor was reported [2, 9,10,12], and the Lyapunov exponent was also computed [10]. Further, oscillatory solutions were investigated and shown to be a generic example of the system permitting escape from a symmetric potential well [14]. As to the rotating modes, unstable periodic orbits were analyzed numerically and experimentally [15], whereas the intermittent region with a large chaotic attractor was used to locate sub-harmonic orbits [16].

The full understanding of the underlying dynamics of the parametric pendulum is still far from complete. In a recent study of the system with weak dissipation, the possibility of three types of chaotic motion has been pointed out: oscillating chaos, rotating chaos, and tumbling chaos. Among these, tumbling chaos appears to be ubiquitous [17]. On the other hand, oscillatory and rotating chaos have been observed in regions of the parameter space which are too small to be identified unambiguously. Hence, the possibility and the mechanism of different types of onset depending on the amplitude of parametric forcing have not been fully explored, al-

*Present address: Department of Physics, University of Illinois, Champaign, IL 61801, U.S.A.

†E-mail: swan@postech.ac.kr

though it has been speculated that an increase of the driving force can have effects analogous to a decrease in damping, such as to result in an attractor merging crisis [18]. As noted, there is a close correspondence between these chaotic phases and the dynamical states of a Josephson junction with different voltage drops or different firing states of a neuron. The parametric oscillator can thus serve as a good model system to study the mechanism of various types of onset also observed in related problems of Josephson junctions or neurons under stimuli, which has been the subject of great interest recently.

Our prime focus in the present work is to understand how a typical nonlinear system such as the parametric oscillator exhibits different types of rotational onset, by using the rotational number approach in combination with bifurcation diagrams [19]. We use the rotation number as an order parameter to characterize distinct chaotic states and present a detailed study of diverse onset mechanisms exhibited by the parametric pendulum in the presence of moderate dissipation, as well as the quantitative nature of each chaotic states. The system is observed to follow two different typical routes to tumbling chaos: one is to successively undergo a hysteretic onset from oscillating chaos to periodic rotation due to bistability and a non-hysteretic onset from rotational chaos to tumbling chaos. The investigation of power spectra, together with the measurement of dimensions of the attractors and of the basin boundary, reveals the onset mechanism of the latter to be an attractor merging crisis. In addition, there also exists another typical route via which the system exhibits a direct onset from periodic oscillation to tumbling chaos, arising from a tangency crisis.

This paper consists of four sections: Section II introduces the system and presents the phase diagram obtained from consideration of the rotation number. Three different chaotic states are identified according to the rotation number, and sections of the phase diagram at certain forcing frequencies with two typical routes are also displayed. Section III is devoted to the study of the mechanism of various onsets which appear in the two sections of the phase diagram. Investigation is carried out by means of bifurcation diagrams, Poincaré sections, and basins of attraction. The correlation dimension of the chaotic attractor and the uncertainty dimension of the basin boundary are also calculated. Additionally, the intermittent mode after the crisis is examined, and the power spectrum right after the crisis is observed to scale approximately as $1/f$ over several decades in the frequency f . Finally, a brief summary is given in Section IV.

II. ROTATION NUMBER AND PHASE DIAGRAM

The parametric pendulum is described by the second-order non-autonomous ordinary differential equation in dimensionless form [1]

$$\frac{d^2\theta}{dt^2} + q\frac{d\theta}{dt} + (1 + 2F \sin \Omega t) \sin \theta = 0, \quad (1)$$

where θ represents the angular position, q the damping coefficient, F the forcing amplitude, and Ω the forcing frequency. Equation (1) can be reduced to a set of coupled first-order equations:

$$\begin{aligned} \frac{d\theta}{dt} &= \omega \\ \frac{d\omega}{dt} &= -q\omega - (1 + 2F \sin \Omega t) \sin \theta, \end{aligned} \quad (2)$$

which constitute the equations of motion governing the time evolution of the system.

In search of different types of onset, we calculate the rotation number

$$\rho \equiv \frac{\langle \dot{\theta} \rangle}{\Omega} = \lim_{t \rightarrow \infty} \frac{\theta(t) - \theta(0)}{\Omega t}, \quad (3)$$

as the parameters are varied in a region of the F - Ω parameter space. It is obvious that the rotation number ρ vanishes identically for periodic oscillations and takes non-zero values for periodic rotations. In the realm of chaos, the behavior of the rotation number also characterizes three types of chaos [19]:

1. *Oscillating chaos.* The rotation number is well defined to be identically zero, *i.e.* $\rho = 0$.
2. *Rotating chaos.* The rotation number has a well defined non-zero value, *i.e.* $\rho \neq 0$.
3. *Tumbling chaos.* The rotation number is not well defined, exhibiting fluctuations. Instead, one may define the *rotation interval* of non-zero measure, within which the rotation number fluctuates.

Accordingly, one can obtain the phase diagram in the parameter space by measuring the rotation number with the parameters varied in appropriate ranges.

In the numerical calculation presented here, we evaluate the rotation number approximately according to $\rho \approx \rho_n \equiv (nT)^{-1}[\theta(nT) - \theta(0)]$ with $T \equiv 2\pi/\Omega$ and for a large integer n . To obtain the phase diagram, we integrate Eq. (2) numerically for $n = 500$ periods via the fourth-order Runge-Kutta algorithm with double-precision arithmetic (15 significant digits) and each forcing period divided into 100 time steps. Then ρ_n is computed on the 400×400 grid of the forcing amplitude F and frequency Ω , after the transient data during the first 200 forcing periods have been discarded, for the system to reach stationarity. Here, the ranges of the parameters are chosen to match those in existing numerical studies cited before, while the damping coefficient is fixed at $q = 0.2$. Note the rather large value of q compared with the value adopted in the existing work [17]; this helps to

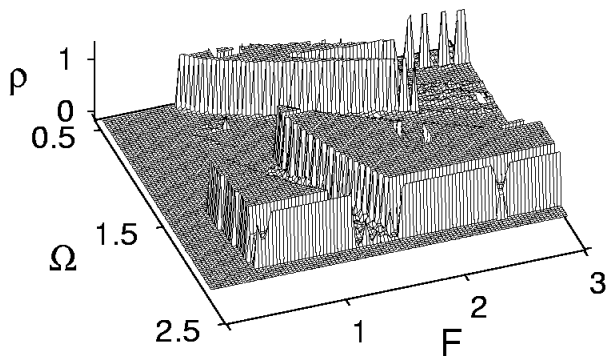


Fig. 1. Rotation number ρ on the F - Ω plane, displaying various types of onset: periodic oscillation \rightarrow oscillating chaos; periodic rotation \rightarrow rotating chaos \rightarrow tumbling chaos; periodic rotation \rightarrow tumbling chaos.

manifest rotating and oscillating chaos more clearly and allows a study of the nature of different types of onset.

The phase diagram obtained in this way is shown in Fig. 1, where plateaus of zero and non-zero heights represent oscillatory and rotational motions, respectively. Although the rotation number alone does not distinguish chaotic motion from periodic motion, it still gives enough information on different types of onset present. For example, the appearance of tumbling chaos is represented by the wiggling region in Fig. 1. Comparing this with the zones of chaotic behavior for smaller damping shown in Fig. 5 of Ref. 17, one observes that qualitative features of the two figures coincide and the primary mode-locked state occupies a wide region. On the other hand, the region of tumbling chaos with windows of other stable motions has a more complex structure than the robust zone of tumbling chaos. Indeed, Fig. 1 exhibits quite complex structure consisting of rotating and tumbling chaos together with oscillating motion in the zone of low forcing frequencies ($\Omega \lesssim 1.0$); this region has not been explored in Ref. 17. Furthermore, close observation of Fig. 1 reveals the existence of two different types of onset leading to tumbling chaos, as the forcing amplitude F is increased at constant forcing frequency Ω : (1) Succession of a hysteretic onset from oscillatory chaos to periodic rotation due to bistability and a non-hysteretic onset from rotational chaos to tumbling chaos; (2) Direct onset from periodic oscillation to tumbling chaos. The former is displayed in Fig. 2(a), corresponding to the section of the phase diagram at $\Omega = 2.0$, whereas the section at $\Omega = 0.732$, shown in Fig. 2(b), displays the latter.

III. CHAOTIC TRANSITIONS

To investigate the nature of the two types of onset observed in Sec. II, in this section we examine bifurcation diagrams along the corresponding sections of the

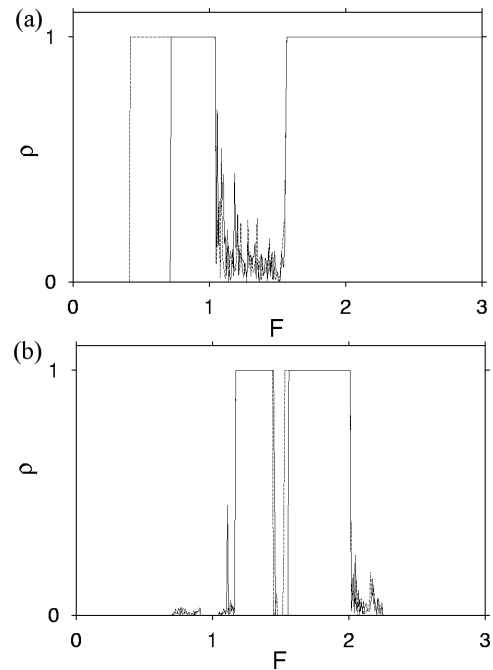


Fig. 2. Rotation number ρ versus forcing amplitude F , obtained from sections of the phase diagram in Fig. 1. Solid and dashed lines represent the behavior as F is raised and reduced, respectively. Observed are different types of rotational onset for (a) $\Omega = 2.0$ and (b) $\Omega = 0.732$.

phase diagram and analyze the attractors in the phase space. We first look into the section $\Omega = 2.0$, where the first type of onset is observed. To obtain the bifurcation diagram, we again integrate Eq. (2) numerically at each value of F , discarding the transient data during the first 500 periods until the system reaches the stationary state. The angular speed ω is then recorded whenever Ωt becomes an integer multiple of 2π during the next 500 periods.

Figure 3 displays the resulting bifurcation diagram at $\Omega = 2.0$. As the forcing amplitude F is increased, a symmetry-breaking pitchfork bifurcation occurs at $F = 0.66463$ after the period-doubling bifurcation to the period-two oscillation, and the stable orbit leads to oscillatory chaos through the typical period-doubling cascade. Note also the presence of the bistability between the oscillation undergoing the cascade and the periodic rotation, the broken-symmetry state in the region $0.41680 < F < 0.71722$, which results in a hysteretic onset. The bistable periodic rotation and the cascade to oscillating chaos are shown in more detail in the insets of Fig. 3. The broken-symmetry rotating solution undergoes a period-doubling cascade to rotating chaos, which grows in size with the forcing amplitude, and finally collides with the chaotic saddle at $F = 1.03659$. At this point both of the two symmetry-related rotating chaotic attractors become meta-stable and all three sets merge to a tumbling chaotic attractor. Hence the onset mecha-

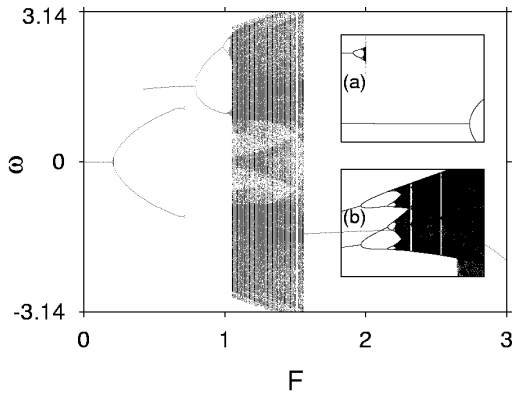


Fig. 3. Bifurcation diagram for $\Omega = 2.0$. The system undergoes a succession of hysteretic onset from oscillating chaos to periodic rotation and non-hysteretic onset from rotating chaos to tumbling chaos. The details of the two onsets are illustrated in the two magnified insets (a) and (b) with no scales, respectively. Note that in (a) the conjugate attractor under reflection symmetry is shown instead.

nism from rotating chaos to tumbling chaos turns out to be the attractor merging crisis [20]. A similar transition from chaotic rotation to tumbling chaos has also been explored in the context of symmetry-restoring attractor merging crisis for a magnetic pendulum with a zero dc component [4].

To obtain the chaotic attractor, we integrate Eq. (2) from an arbitrary initial condition over 500 forcing periods and plot the Poincaré sections taken at $\Omega t = 0 \pmod{2\pi}$, after the first 100 periods. The resulting figure shows the tumbling chaotic attractor in thick points in Fig. 4(a), which contains a large number of points corresponding to the intermittent motion of the system between the precrisis chaotic saddle and two small precrisis rotating chaotic attractors in addition to the three chaotic sets themselves. This verifies the speculation in Ref. [18] that the system will experience an attractor merging crisis if the driving force is varied instead of damping, with a larger driving force playing the role of low damping. The correlation dimension [21] of the tumbling chaotic attractor right after the crisis, shown in Fig. 4(a), is calculated to be $d = 1.37 \pm 0.03$, which is substantially larger than the dimension $d = 1.24 \pm 0.08$ of the rotating chaotic attractor just before the crisis at $F = 1.036$. We also performed similar simulations starting from the initial conditions on the 230×200 grid in (θ, ω) , where the computation of short-term rotations reveals no correlated structure in the phase space. The well-known crisis-induced intermittency, namely, the characteristic temporal behavior of intermittent switching [20] between precrisis attractors accompanied by the attractor merging crisis, is also observed here and the power spectrum right after the crisis exhibits $1/f$ -dependence, as shown in Fig. 4(b). The least-square fit to the form $f^{-\alpha}$ gives the exponent $\alpha = 1.026 \pm 0.001$ at low frequencies, over more than two

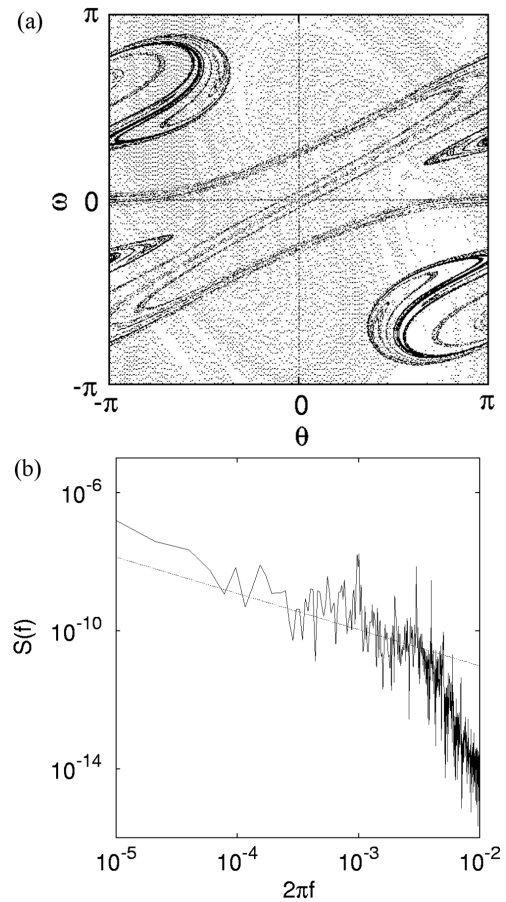


Fig. 4. Tumbling chaos at $F = 1.0367$ in the phase space and the corresponding power spectrum. (a) The tumbling chaotic attractor is shown in thick points. The gray points denote those for short-term clockwise rotation, which reveal no correlated structure. (b) The power spectrum $S(f)$ right after the crisis displays $1/f$ behavior for more than two decades in frequency f . The slope of the dotted line is unity.

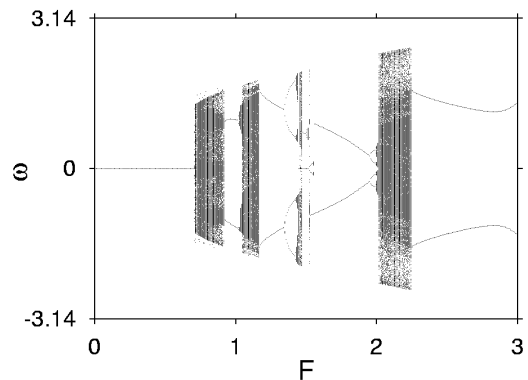


Fig. 5. Bifurcation diagram for $\Omega = 0.732$. The system undergoes a non-hysteretic direct onset from periodic oscillation to tumbling chaos.

decades in frequency f .

We now examine the section $\Omega = 0.732$, where the

second type of onset is observed. Figure 5 displays the bifurcation diagram at $\Omega = 0.732$, which is obtained in the same manner as Fig. 3. Although we are unable to decide from the bifurcation diagram whether the chaotic state in the region $0.7125 < F < 0.9160$ corresponds to tumbling chaos or oscillating chaos, fluctuations of the rotation number observed in the same region of Fig. 1 indicate that the onset at $F = 0.7125$ is actually a direct one. The mechanism of this direct onset appears to be the heteroclinic tangency crisis due to the tangency of the stable manifold and the unstable manifold of unstable periodic orbits $(0, -\pi)$ and $(0, \pi)$. The bifurcation diagram also reveals that, instead of being predominant after the onset, tumbling chaos is apparent only in rather narrow regions between oscillations or rotations, reflecting the complex structure of the phase diagram. Tumbling chaotic regions always give ways to periodic rotations or oscillations due to the boundary crisis, while they emerge via the interior crisis or the attractor merging crisis.

IV. SUMMARY

A damped parametrically forced pendulum is a classical example of the forced nonlinear oscillator, and its behavior represents a large class of systems including the magnetic pendulum in a dc and ac magnetic field and related problems of driven Josephson junctions and neurons under stimuli. We have studied different types of possible onset in the parametrically forced pendulum, as the forcing amplitude is increased. It has been noted that the rotation number may be taken as an order parameter characterizing different types of chaos, which can be further clarified in combination with the analysis of bifurcation diagrams.

Accordingly, the phase diagram has been empirically obtained from the efficient computation of the rotation number. This reveals the complex structure in the region of low forcing frequencies, previously regarded as the zone of tumbling chaos, together with the existence of two types of onset. Each of the onsets has been examined by means of the bifurcation diagram, with the forcing frequency fixed at values for typical behavior: $\Omega = 2.0$ and $\Omega = 0.732$. At $\Omega = 2.0$, the system has been observed to undergo two successive onsets, one from oscillating chaos to periodic rotation and the other from rotating chaos to tumbling chaos. The former is a hysteretic onset due to bistability, whereas the non-hysteretic onset mechanism of the latter turns out to be an attractor merging crisis. Between these onsets, there are period-doubling bifurcations to oscillating or rotating chaos. The correlation dimension of the attractors was measured before and after the crisis. In addition, the power spectrum right after the crisis, where the crisis-induced intermittency is manifested, has been found to display $1/f$ behavior for more than two decades. At $\Omega = 0.732$, on the other hand, the system experiences a direct onset from peri-

odic oscillations to tumbling chaos, the onset mechanism of which turns out to be a heteroclinic tangency crisis. However, tumbling chaos is not robust after the onset: Regions of oscillations or rotations are widely found, due to the boundary crisis, and tumbling chaos occupies only rather narrow regions in between. Further investigation is needed to obtain a full understanding of such a complex structure in the phase diagram.

ACKNOWLEDGMENTS

We thank H. Kook and the referee for helpful suggestions and acknowledge the partial support from the Ministry of Science and Technology through the National Research Laboratory Program and the Ministry of Education through the Brain Korea 21 Program.

REFERENCES

- [1] L. D. Landau and E. M. Lifshitz, *Mechanics* (Pergamon Press, New York, 1976).
- [2] S.-Y. Kim and K. Lee, *Phys. Rev. E* **53**, 1579 (1996).
- [3] S.-Y. Kim, S.-H. Shin, J. Yi and C. Jang, *Phys. Rev. E* **56**, 6613 (1997).
- [4] S.-Y. Kim, *J. Phys. A* **32**, 6727 (1999).
- [5] D. E. McCumber, *J. Appl. Phys.* **39**, 3113(1968); W. C. Stewart, *Appl. Phys. Lett. B* **12**, 277 (1968).
- [6] W. G. Choe and S. Kim, *J. Korean Phys. Soc.* **26**, S382 (1993).
- [7] K. Aihara, T. Numajiri, G. Matsumoto and M. Kotani, *Phys. Lett. A* **116**, 313 (1986).
- [8] M. Park and S. Kim, *J. Korean Phys. Soc.* **29**, 9 (1996).
- [9] J. B. McLaughlin, *J. Stat. Phys.* **24**, 375 (1981).
- [10] R. W. Leven and B. P. Koch, *Phys. Lett. A* **86**, 71 (1981).
- [11] B. P. Koch and R. W. Leven, *Physica D* **16**, 1 (1985).
- [12] B. P. Koch, R. W. Leven, B. Pompe and C. Wilke, *Phys. Lett. A* **96**, 219 (1983).
- [13] R. W. Leven, B. Pompe, C. Wilke and B. P. Koch, *Physica D* **16**, 371 (1985).
- [14] M. J. Clifford and S. R. Bishop, *Phys. Lett. A* **184**, 57 (1993).
- [15] W. van de Water and M. Hoppenbrouwers, *Phys. Rev. A* **44**, 6388 (1991).
- [16] M. J. Clifford and S. R. Bishop, *Phys. Lett. A* **201**, 191 (1995).
- [17] S. R. Bishop and M. J. Clifford, *J. Sound and Vib.* **189**, 142 (1996).
- [18] R. W. Leven, M. Selent and D. Uhrlandt, *Chaos, Solitons and Fractals* **45**, 661 (1993).
- [19] C. Baesens, S. Kim, R. S. MacKay and J. Guckenheimer, *Physica D* **49**, 387 (1991).
- [20] C. Grebogi, E. Ott, F. Romerías and J. A. Yorke, *Phys. Rev. A* **36**, 5365 (1987).
- [21] P. Grassberger and I. Procaccia, *Phys. Rev. Lett.* **50**, 346 (1983).
- [22] E. Ott, *Chaos in Dynamical Systems* (Cambridge University Press, Cambridge, 1993).